




Growth and composition of an ultrathin Ba-Ti-O quasicrystal film and its crystalline approximant on Pt(111)

Junji Yuhara ^{*}, Keito Horiba, Ryoichi Sugiura, Xu Li , and Tomoaki Yamada
Graduate School of Engineering, Nagoya University, Nagoya 464-8603, Japan

 (Received 2 May 2020; revised 20 August 2020; accepted 25 September 2020; published 16 October 2020)

As a new family of quasicrystals, oxide quasicrystals (OQCs) were recently discovered in Ba-Ti-O films on Pt(111). Here we report on the growth and composition of an ultrathin Ba-Ti-O OQC film and its crystalline approximant, studied by scanning tunneling microscopy (STM), low-energy electron diffraction, Auger electron spectroscopy, x-ray photoelectron spectroscopy, and Rutherford backscattering spectroscopy. STM images reveal a wide-scale ultrathin OQC film without BaO islands, and magnified STM images display typical OQC clusters. The ultrathin OQC film has been prepared by annealing an oxide crystalline approximant with decreasing Ti concentration. We also found that the ultrathin Ba-Ti-O film forms a (2×2) superstructure on annealing the ultrathin OQC film. For quantitative analysis, the XPS peak intensity was measured as a function of elemental atomic density. The elemental atomic densities for the ultrathin OQC film were determined to be 8×10^{14} , 4×10^{14} , and 3×10^{14} atoms/cm² for Ba, Ti, and O, respectively.

DOI: [10.1103/PhysRevMaterials.4.103402](https://doi.org/10.1103/PhysRevMaterials.4.103402)

I. INTRODUCTION

As a new family of quasicrystals (QCs), ultrathin oxide quasicrystal (OQC) films on Pt(111) were discovered by Förster in 2013 [1]. Identifying the geometrical structure is an inevitable challenge not only for fundamental studies of this material's unique chemical and physical properties, but also for industrial applications. In general, QC structures can be expressed as cluster tiling. The clusters are arranged quasiperiodically for a QC, while clusters are arranged periodically for a crystalline approximant. Structural analysis of the clusters in a crystalline approximant is the first step in determining the QC geometrical structure, as it is easier to perform density functional theory (DFT) simulations and diffraction experiments because of the periodicity of the approximant.

Thus far, ultrathin Ba-Ti-O OQC films on Pt(111) have exhibited a unique cluster in scanning tunneling microscopy (STM) images [1]. In contrast, several types of clusters are observed for the ultrathin Ba-Ti-O oxide crystalline approximant (OCA) on Pt(111) [2–6]. One of the OCA clusters, the so-called sigma phase, is locally observed in the OQC domain at the STM images [5]. To experimentally determine the atomic arrangement, it is desirable to grow a wide-scale OCA film. In addition, to identify a structural model through DFT calculations or experimental diffraction techniques, it is useful to determine the elemental atomic density for OCA and OQC films.

Structural models can be proposed via DFT calculations based on the square-triangle-rhombus model, the so-called Niizeki-Gähler tiling [7,8], because STM results indicate that the cluster type is square-triangle-rhombus. From the Niizeki-Gähler tiling model, the composition is calculated to

be Ba_{0.37}TiO_{1.55}. The calculated Ba/Ti ratios range from 0.23 to 0.50 for a variety of crystalline approximants including squares, triangles, and rhombuses, assuming square unit cells (side length of 49.4 Å) [9].

Two experimental studies have been reported for OCA films, whose clusters differ from the OQC clusters, and the average stoichiometry has been estimated as Ba₄Ti₄O₁₀ based on a combined analysis of STM, surface x-ray diffraction, and DFT calculations [3,10]. In this OCA model, the Ba atoms and some of the O ions buckle outward from the surface. In contrast, the same group has also reported that the Ti atoms buckle outward instead of Ba and O [11], based on a combination of STM and noncontact atomic force microscopy (nc AFM).

In this work, we report the epitaxial growth of well-ordered, large-area, ultrathin Ba-Ti-O films on Pt(111), changing from the OCA phase into the OQC phase and a (2×2) periodic structure on annealing. We examined the elemental atomic density of Ba, Ti, and O by STM, low-energy electron diffraction (LEED), Auger electron spectroscopy (AES), and x-ray photoelectron spectroscopy (XPS). For quantitative analysis, Rutherford backscattering spectroscopy (RBS) was employed to obtain calibration XPS intensity curves as a function of elemental atomic density [12].

II. EXPERIMENT

The experiments were performed using an ultrahigh-vacuum (UHV) system at Nagoya University. The system consisted of a preparation chamber with a base pressure below 5×10^{-10} mbar and an analysis chamber with a base pressure below 10^{-10} mbar. The system was equipped with a rearview LEED system operating with a LaB₆ filament and a room-temperature (RT) STM system (Omicron STM-1). All STM images were acquired with W tips and electrochemically etched in a KOH solution, in constant current mode. The AES

^{*}j-yuhara@energy.nagoya-u.ac.jp

and XPS spectra were recorded with a VG Clam II spherical electrostatic analyzer using conventional pass energy modes with a constant retarding ratio (10) and constant analyzing energy (10 eV), using an electron gun ($E_p = 3$ keV) and a Mg $K\alpha$ x-ray source ($h\nu = 1253.6$ eV) as the incident beam, respectively. The compositional ratios were calculated from AES spectra with reference to the AES handbook [13], using elemental sensitivity factors of 0.125 for Ba-*MNN* (584 eV), 0.44 for Ti-*LMM* (418 eV), and 0.5 for O-*KLL* (503 eV). The elemental sensitivity factors in the handbook are specific for a cylindrical mirror analyzer, not for a spherical analyzer. Therefore, the AES spectra were used to examine the reproducibility and to conduct a semiquantitative analysis. The overall resolution of the spectrometer for XPS spectra was 0.1 eV.

Clean Pt(111) surfaces were prepared by 2-keV Ar^+ ion sputtering at RT, followed by annealing at 600 °C with electron bombardment of the sample holder. The sample temperature was monitored with a radiation thermometer and a type-K thermocouple mounted on the base plate of the sample holder. The purity of the surface was measured by AES after sputtering and annealing; no contaminants were observed within the detection limits, while a sharp (1 × 1) LEED pattern was observed.

Ultrathin Ba-Ti-O films with a uniform thickness of 2 nm were prepared on Pt(111) by *ex situ* using a high-vacuum pulsed laser deposition (PLD) chamber. The O_2 gas partial pressure during PLD growth was 40 mbar. The details of the PLD equipment have been described in a previous report [14]. The specimens were transferred to the UHV chamber and annealed at a temperature of 850 °C–1050 °C in UHV or at 600 °C in an O atmosphere of 3×10^{-6} mbar in order to control the film composition. If the Ba concentration was too high, the Ba-Ti-O films formed monoatomic Ba-Ti-O films with three-dimensional (3D) Ba-Ti-O islands. Because the Ba concentration did not change upon the annealing, the specimens were sputtered by Ar^+ ions at RT and postannealing. The monoatomic Ba-Ti-O films were sputtered and the Ba and Ti atoms were migrated from 3D Ba-Ti-O islands into the terrace on annealing. If the Ti concentration decreased too much upon annealing, Ti was supplied for 0.9 ML, confirmed by RBS, by physical vapor deposition from an electron bombardment evaporator in the UHV chamber. We define 1 ML as an overlayer with the atomic density of the Pt(111) layer: 1.5×10^{15} atoms/cm². The sample preparation process is illustrated in Fig. 1.

The RBS spectra were acquired in a conventional high-vacuum chamber, which was evacuated to a base pressure of less than 2×10^{-6} mbar and equipped with a manipulator for mounting specimens and a silicon surface barrier solid-state detector. The chamber was connected through a differentially pumped space to a beam line of a 2-MeV Van de Graaff accelerator [15]. The incident He^+ ion beam energy was 1.5 MeV. Specimens of ultrathin Ba-Ti-O films with varying thickness were prepared on graphite in a PLD chamber for quantitative analysis. The elemental concentration was estimated from RBS spectra with an accuracy of 10%, and the depth resolution was approximately 10 nm. Details regarding the experimental setup for RBS have been published elsewhere [16].

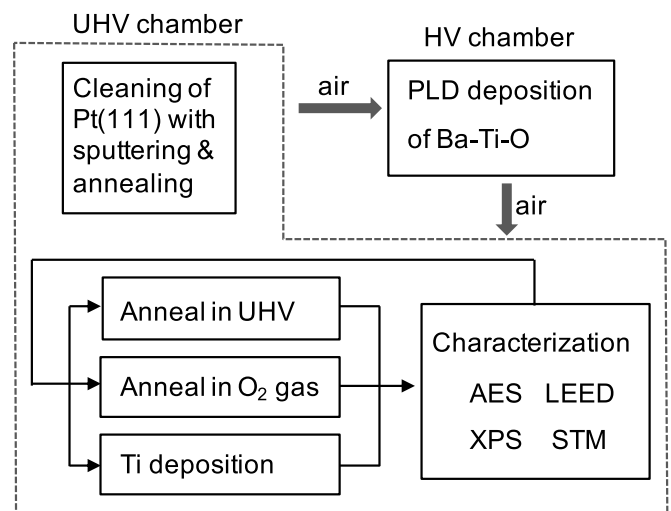


FIG. 1. Procedure for preparing ultrathin Ba-Ti-O films for QC, crystalline approximant, and superstructure on Pt(111).

III. EXPERIMENTAL RESULTS AND DISCUSSION

Figures 2(a)–2(c) show LEED patterns of the OCA, OQC, and periodic superstructure of ultrathin Ba-Ti-O films on Pt(111), acquired at a primary electron energy of 66 eV. The LEED patterns exhibit primitive (1 × 1) spots originating from Pt(111) for each specimen in addition to unique diffraction spots. The LEED pattern of OCA, shown in Fig. 2(a), is in good agreement with previous reports [1,10]. The difference between both patterns originates from the different kinetic energy of the incident electron beam. The OCA film transforms to the OQC film upon annealing at 1000 °C for 5 min with decreasing Ti concentration. The OQC LEED pattern displayed in Fig. 2(b) is consistent with a previously reported OQC LEED pattern [1]. The OQC films are transformed into a (2 × 2) periodic structure upon annealing at 1000 °C for 5 min, as shown in Fig. 2(c). The primitive spots are very sharp without any splitting. It is reported that BaTiO_3 islands exhibit a LEED pattern of $\text{BaTiO}_3(111)(1 \times 1)$ and the second order of $\text{BaTiO}_3(111)$ primitive spots is 2% smaller than Pt(111) primitive spots [1,4,17], which leads to splitting of the first order of Pt primitive spots. Therefore, the (2 × 2) sharp LEED pattern clearly indicates that there are no islands. In the direct observation using the wide-scale STM image, no islands, such as BaO or BaTiO_3 islands, were observed, as shown in Fig. 2(d). Notably, magnified STM images of the OQC film exhibit a highly quasiperiodic structure, as shown in Fig. 2(e). Figure 2(f) shows typical AES spectra for the Ba-Ti-O film on Pt(111) prepared on UHV annealing at 600 °C for 5 min as well as the OCA, OQC, and (2 × 2) films. For the Ba-Ti-O film, Ba, Ti, and O peaks are observed while Pt signals at 64 and 43 eV interfere with Ba signals at 73 and 47 eV because of the Ba-Ti-O film that is 2 nm in thickness. However, Pt signals at higher energies at 237 and 168 eV, a relatively larger electron mean free path, are clearly observed. For the OCA, OQC, and (2 × 2) films, the AES peak from the Pt substrate (64 eV) is clearly present, and Ba, Ti, and O peaks are decreased but clearly recognized. Thus, Ba, Ti, and O atoms are considered to be submonolayer regimes. From the AES spectrum

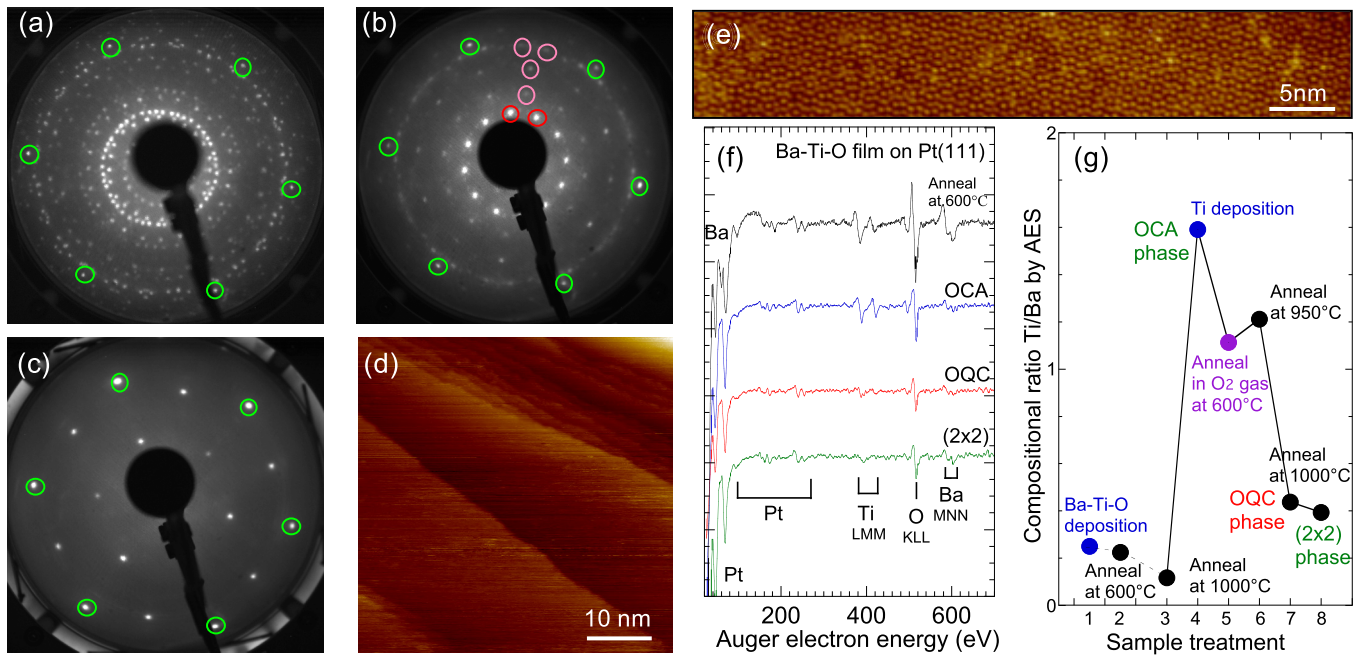


FIG. 2. LEED patterns of ultrathin Ba-Ti-O films for (a) crystalline approximant, (b) QC, and (c) (2×2) superstructure on Pt(111). The incident electron energy is 66 eV. The Pt(111) primitive spots (green circles) are marked in the image. (d) Wide-scale STM image of the OQC film. (e) Wide-scale high-resolution STM image of the OQC film. (f) AES spectra of the Ba-Ti-O films on Pt(111) on annealing at 600 °C as well as those at (a)–(c). (g) The Ti/Ba compositional ratio determined by AES as a function of sample treatment.

for the OQC film, the compositional ratio is calculated to be Ba:Ti:O = 9:2:7. It is clearly seen that Ti signal intensity decreased for the OQC to (2×2) films in comparison with the OCA film. Figure 2(g) shows a Ti/Ba compositional ratio determined by AES as a function of sample treatment. For the

Ti/Ba compositional ratio of 0.2–0.5, the OQC LEED patterns shown in Fig. 2(b) are observed. When the compositional ratio exceeds 0.5, the OCA LEED patterns are observed. Therefore, the Ti atomic density is directly related to the origin of the OCA and OQC. When the compositional ratio is lower than

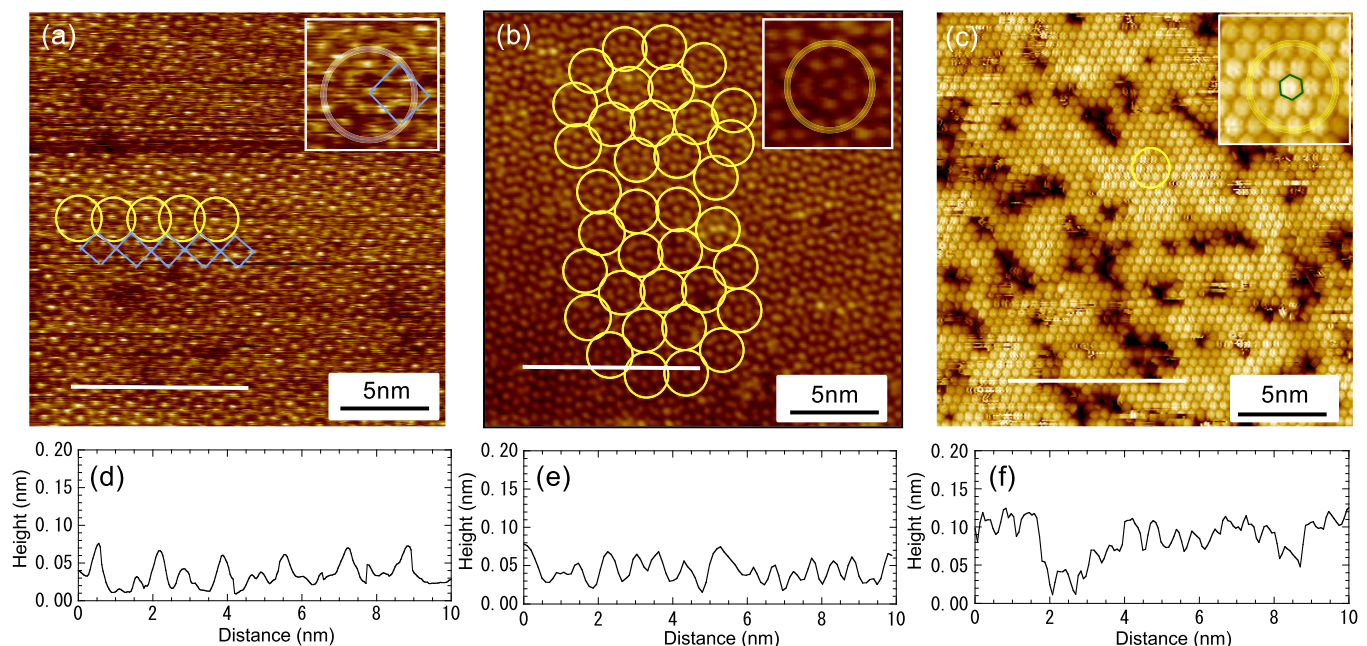


FIG. 3. STM images of ultra-thin Ba-Ti-O films for (a) crystalline approximant, (b) QC, and (c) (2×2) superstructure on Pt(111). The images were recorded in constant current mode with a tunneling current of 700 pA and a sample bias voltage of +1.0 V. The insets present magnified STM images of basic clusters and the superstructure. Unit cells of sigma phase are marked in (a). (d)–(f) Section profiles along the lines marked in the STM images at (a)–(c).

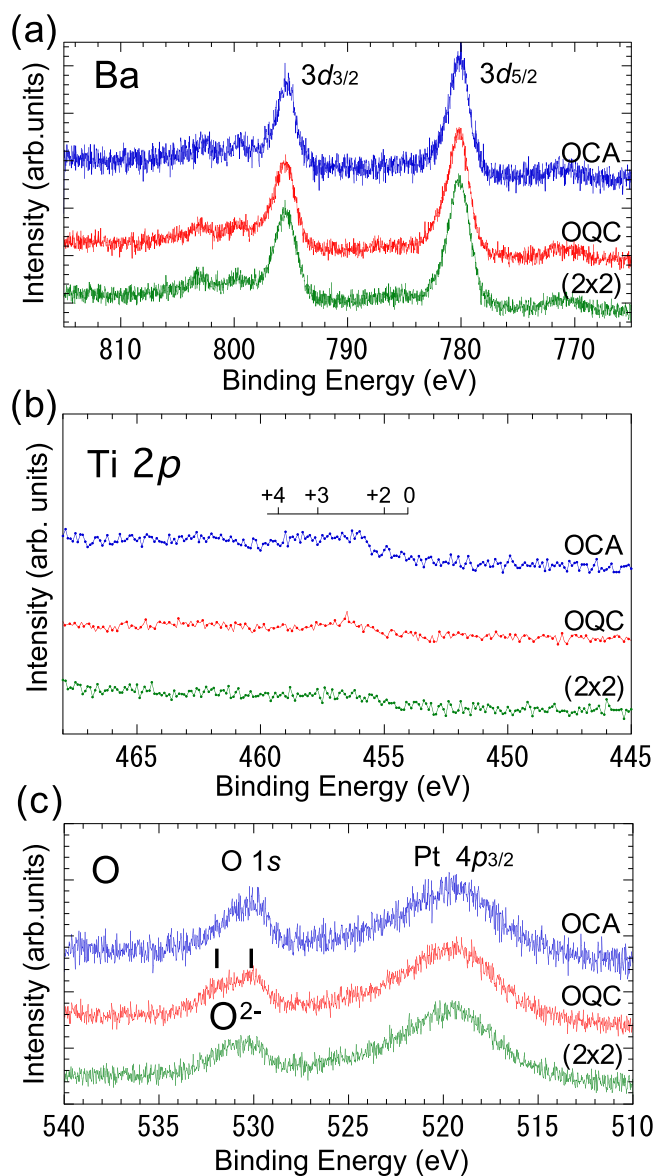


FIG. 4. XPS spectra of (a) Ba $3d$, (b) Ti $2p$, and (c) O $1s$ for ultrathin Ba-Ti-O films in crystalline approximant, QC, and (2×2) superstructure on Pt(111).

0.2, the (2×2) periodic structure is observed in the LEED pattern.

Figures 3(a)–3(c) show STM images for the OCA, OQC, and (2×2) periodic superstructure samples, with their section profiles shown in Figs. 3(d)–3(f), respectively. In the STM image of the OCA film, there are clusters that are identical to previous reports, the so-called sigma phase, [1,10]. From the section profile, the periodicity is calculated to be 1.7 nm, corresponding to the diagonal of the unit cell of 1.8 nm [1,10]. The areal density of maxima for the OCA is calculated at $2.5 \times 10^{14} \text{ cm}^{-2}$. The OCA films transform into an OQC film and finally exhibit a (2×2) periodic superstructure on annealing, but the reverse process is not observed. When Ti atoms with 0.5 ML coverage are deposited onto the (2×2) film, OCA or OQC films are formed upon annealing. The areal density of maxima for the OQC is calculated at $3.2 \times 10^{14} \text{ cm}^{-2}$, which

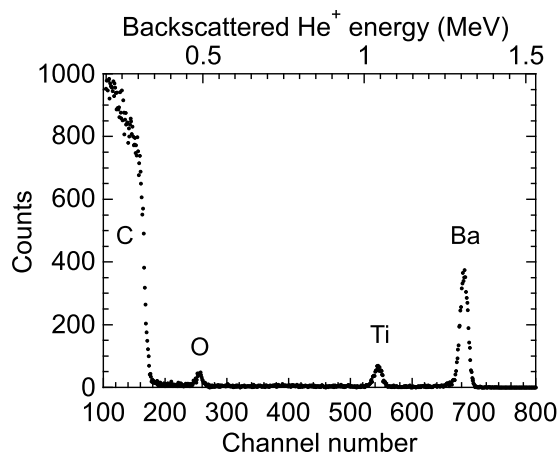


FIG. 5. RBS spectrum of an ultrathin Ba-Ti-O film on graphite.

is 30% higher than the OCA surface. As reported by Förster *et al.*, the OQC surface forms square-triangle-tiling and the OCA surface forms square-triangle tiling [1,10]; the maxima density is strongly related to the tiling. From the section profiles, the maxima have a height of 0.04 ± 0.01 nm for the OCA and OQC films, indicating an atomically flat layer. The maxima may originate from a specific chemical species. For the (2×2) periodic superstructure, the surface exhibits rather small height fluctuations, which are estimated to be approximately 0.1 nm. Magnified STM images show unique pentagon motifs for each (2×2) unit cell. The width of the pentagon motif is ~ 0.45 nm, which is considerably larger than the atomic size. The areal density of the pentagon motif is calculated to be $3.8 \times 10^{14} \text{ cm}^{-2}$.

Figure 4 shows XPS spectra of the OCA, OQC, and (2×2) films for the Ba $3d$, Ti $2p$, and O $1s$ core levels. The Ba binding energy is determined to be 780.1 eV, which is consistent with previous findings [1]. Because the binding energies for metallic Ba and Ba^{2+} are 779.3 and 779.1 eV, respectively [18], the Ba atoms may be metallic instead of the Ba^{2+} ion. The O $1s$ intensity is found to be much lower than that reported in a previous study, which reported BaTiO_3 islands on a terrace, based on the peak intensity ratio O/Pt [1]. Therefore, both XPS spectra and wide-scale STM images confirm an absence of BaTiO_3 islands. The oxygen peak consists of two components, especially for the OQC film. Because the LEED pattern only shows the OQC spots, there are two occupation sites for O ions. In the present study, Ti $2p$ intensity is also much lower than the previous reports that the Ti^{3+} signal arises from the rewetting layer while the Ti^{4+} signal originates from BaTiO_3 islands [19]. The binding energies for metallic Ti, Ti^{2+} , Ti^{3+} ion, and Ti^{4+} ion are reported to be 454, 455, 458, and 459 eV [20]. Here, Ti shows a small peak at 456.5 eV for the OQC film, whose binding energy is in between Ti^{2+} and Ti^{3+} . Therefore, the Ti might be the Ti^{2+} ion. For the OCA film, Ti has a wider peak at 456–458 eV, possibly a mixture of Ti^{2+} and Ti^{3+} ions. Thus, there are a few occupation sites for Ti ions.

Figure 5 shows a typical RBS spectrum of a Ba-Ti-O film on graphite. Each elemental component was quantitatively calculated using the graphite signal intensity.

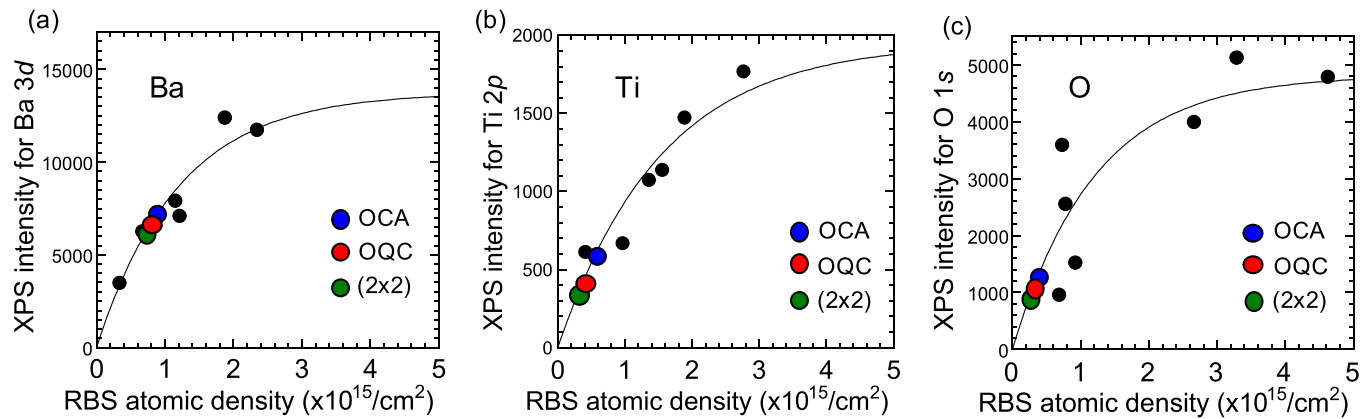


FIG. 6. XPS intensity of (a) Ba $3d$, (b) Ti $2p$, and (c) O $1s$ for ultrathin Ba-Ti-O films as a function of the elemental atomic density estimated from RBS spectra. The OCA, OQC, and (2×2) superstructure results are marked as blue, red, and green circles, respectively.

Figure 6 shows calibration curves for Ba $3d$, Ti $2p$, and O $1s$ intensities as a function of atomic density, as determined by RBS. We prepared six Ba-Ti-O films on graphite for all different thicknesses; we plotted six black solid circles after the XPS intensity measurements. The calibration curves were determined using the Beer-Lambert law. The elemental atomic density for Ba, Ti, and O atoms in the OQC film was determined to be $(8 \pm 3) \times 10^{14}$, $(4 \pm 2) \times 10^{14}$, and $(3 \pm 1) \times 10^{14}$ atoms/cm², respectively. Since the Ba atoms are possibly assigned to be metallic and the Ti atoms could be Ti²⁺ from XPS analysis, it is proposed that the stoichiometry is Ba:Ti:O = 2:1:1.

For the OCA film, the Ba and O atomic densities are similar to those of the OQC film, but the Ti atomic density is larger at 6×10^{14} atoms/cm². AES compositional analysis also shows a higher Ti/Ba ratio for the OCA film than for the OQC film [Fig. 2(g)]. Therefore, Ti is a key element for differentiating between the two growth modes of the OCA and OQC films.

From the Niizeki-Gähler tiling model, it has been proposed that the composition is calculated to be Ba_{0.37}Ti_{0.55} [9]. In this model, the atomic density is shown to be 2.6×10^{14} atoms/cm² for Ba, 6.9×10^{14} atoms/cm² for Ti, and 11×10^{14} atoms/cm² for O. These values are rather inconsistent with the present results, especially for the Ba and O atomic densities. Experimentally, there is a report for other OCA film using surface x-ray diffraction (SXRD) that the average stoichiometry has been estimated as Ba₄Ti₄O₁₀ in the unit cell of 12.9×13.1 Å [3], whose clusters are rather different from the OQC clusters. In this model, the atomic density has been determined to be 2.4×10^{14} atoms/cm² for Ba and for Ti, and 5.9×10^{14} atoms/cm² for O. The Ba atomic density is quite smaller than the present result (8×10^{14} atoms/cm² for Ba). According to the Niizeki-Gähler tiling model, the maxima in the STM images arise from Ba atoms [9]. On the other hand, it has been reported from SXRD and nc AFM that the maxima arise from Ti atoms [3,9]. In addition, Ti $3d$ states near the Fermi level have been observed by photoemission spectroscopy [18].

Both the AES and XPS results indicate that the Ti atomic density for the OCA film is almost double the value for the OQC film, even though the maxima in the STM images for

the OCA film are 30% lower than the OQC surface, originating from square-triangle tiling and square-triangle-rhombus tiling, respectively. If the maxima arise from Ti atoms, Ti atomic density should increase for 30% for the OQC film. In the present study, the OCA film transforms into the OQC film on annealing with decreasing Ti concentration. Since the SXRD measurement suggests that the maxima are from a high-Z element, the Ba or Ti atomic density for the OCA film determined by RBS-XPS quantitative analysis shows much higher values than those for the maxima density. Therefore, the maxima may arise from a portion of the Ba or Ti atoms for the OCA film.

For the (2×2) periodic superstructure, the areal density of the pentagon motif is calculated to be 3.8×10^{14} cm⁻², while the Ba, Ti, and O atomic densities are determined to be 7×10^{14} , 3×10^{14} , and 3×10^{14} atoms/cm². Therefore, it is considered that there are two Ba atoms, one Ti atom, and one O atom per (2×2) unit cell. Because there is a height fluctuation in the STM images [Fig. 3(c)], the (2×2) domain is an oxide film but locally it may be the metallic state (darker area in STM image).

IV. CONCLUSIONS

We have successfully prepared wide-scale OQC, OCA, and superstructure films without 3D islands. Wide-scale magnified STM images clearly demonstrate that the OQC phase in this work is identical to that of previous reports. The basic clusters observed for the OCA film are identical to those for the OQC film, as confirmed by LEED and STM. Using high-quality specimens, the surface atomic densities for Ba, Ti, and O in the OQC film were determined to be $(8 \pm 3) \times 10^{14}$, $(4 \pm 2) \times 10^{14}$, and $(3 \pm 1) \times 10^{14}$ atoms/cm², respectively.

ACKNOWLEDGMENTS

This work was partially supported by a Grant-in-Aid for Scientific Research on Innovative Areas “Hypermaterials: Innovation of Materials Science in Hyper Space” (Grant No. 20H05267) from the Ministry of Education, Culture, Sports, Science, and Technology (MEXT).

- [1] S. Förster, K. Meinel, R. Hammer, M. Trautmann, and W. Widdra, *Nature* **502**, 215 (2013).
- [2] S. Förster and W. Widdra, *Surf. Sci.* **604**, 2163 (2010).
- [3] S. Förster, M. Trautmann, S. Roy, W. A. Adeagbo, E. M. Zollner, R. Hammer, F. O. Schumann, K. Meinel, S. K. Nayak, K. Mohseni, W. Hergert, H. L. Meyerheim, and W. Widdra, *Phys. Rev. Lett.* **117**, 095501 (2016).
- [4] S. Förster, S. Schenk, E. Maria Zollner, O. Krahn, C.-T. Chiang, F. O. Schumann, A. Bayat, K.-M. Schindler, M. Trautmann, R. Hammer, K. Meinel, W. A. Adeagbo, W. Hergert, J. Ingo Flege, J. Falta, M. Ellguth, C. Tusche, M. DeBoissieu, M. Muntwiler, T. Greber *et al.*, *Phys. Status Solidi B* **257**, 1900624 (2019).
- [5] S. Schenk, E. M. Zollner, O. Krahn, B. Schreck, R. Hammer, S. Förster, and W. Widdra, *Acta Cryst. A* **75**, 307 (2019).
- [6] E. Maria Zollner, F. Schuster, K. Meinel, P. Stötzner, S. Schenk, B. Allner, S. Förster, and W. Widdra, *Phys. Status Solidi B* **257**, 1900655 (2020).
- [7] N. Niizeki and H. Mitani, *J. Phys. A: Math. Gen.* **20**, L405 (1987).
- [8] F. Gähler, in *Quasicrystalline Materials: Proceedings of the I.L.L./Codest Workshop* (World Scientific, Singapore, 1988), pp. 272–284.
- [9] E. Cockayne, M. Mihalkovič, and C. L. Henley, *Phys. Rev. B* **93**, 020101(R) (2016).
- [10] S. Roy, K. Mohseni, S. Förster, M. Trautmann, F. Schumann, E. Zollner, H. Meyerheim, and W. Widdra, *Z. Kristallogr.* **231**, 749 (2016).
- [11] E. M. Zollner, S. Schenk, M. Setvin, and S. Förster, *Phys. Status Solidi B* **257**, 1900620 (2019).
- [12] L. H. Chan and J. Yuhara, *Surf. Sci.* **661**, 69 (2017).
- [13] P. W. Palmberg, G. E. Riach, R. E. Weber, and N. C. MacDonald, *Handbook of Auger Electron Spectroscopy*, 5th ed. (Physical Electronic Industries, Edina, MN, 1972).
- [14] S. Kondo, T. Yamada, A. K. Tagantsev, P. Ma, J. Leuthold, P. Martelli, P. Boffi, M. Martinelli, M. Yoshino, and T. Nagasaki, *Appl. Phys. Lett.* **115**, 092901 (2019).
- [15] J. Yuhara, M. Inoue, and K. Morita, *J. Vac. Sci. Technol. A* **10**, 334 (1992).
- [16] J. Yuhara, K. Morita, J. Falta, B. H. Müller, and M. Horn-von Hoegen, *Surf. Interface Anal.* **31**, 754 (2001).
- [17] S. Förster, J. I. Flege, E. M. Zollner, F. O. Schumann, R. Hammer, A. Bayat, K.-M. Schindler, J. Falta, and W. Widdra, *Ann. Phys.* **529**, 1600250 (2017).
- [18] M. I. Sosulnikov and Y. A. Teterin, *J. Electron Spectrosc. Relat. Phenom.* **59**, 111 (1992).
- [19] S. Förster, K. Meinel, K.-M. Schindler, and W. Widdra, *Surf. Interface Anal.* **44**, 628 (2012).
- [20] V. V. Atuchin, V. G. Kesler, N. V. Pervukhina, and Z. Zhang, *J. Electron Spectrosc. Relat. Phenom.* **152**, 18 (2006).